ACS OMEGA

Open Access

http://pubs.acs.org/journal/acsodf

Article

Light-Responsive Layer-By-Layer Film Containing Gold Nanorods for Sequential Drug Release

Baljinder Singh, Mamta Ramgopal Chejara, and Myoung-Hwan Park*

Cite This: *ACS Omega* 2023, 8, 48405−48412

Read Online

ACCESS | Metrics & More | Article Recommendations | Supporting Information

ABSTRACT: Chemically and physically stable multidrug-loaded layer-by-layer (LbL) films are promising candidates for sequential and on-demand drug release at concentrations suitable for various applications. The synergistic effect of the sequential release of drugs may enhance their therapeutic efficacy in treating skin cancer and other complex medical conditions. In this study, we prepared LbL films by alternating the deposition of cationic linear polyethylenimine, camptothecin (CPT)-loaded gold nanorods (GNRs), anionic poly(styrenesulfonate), and doxorubicin (DOX) based on electrostatic interactions. The film exhibited loading of CPT and DOX, which could be tuned according to the requirements of the application by changing the parameters of the LbL process. Herein, CPT was encapsulated in GNRs and showed good stability and absorption in the near-infrared (NIR) range (650−900 nm). The prepared LbL film showed a pH-dependent DOX release. Subsequently, the functionalized GNRs showed excellent photothermal properties, which assisted the on-demand release of CPT upon NIR irradiation with further release of DOX. Our results suggest that the LbL approach for sequential drug release can be an effective drug delivery platform owing to its cytocompatibility, anticancer effects, and stimuli-responsive properties.

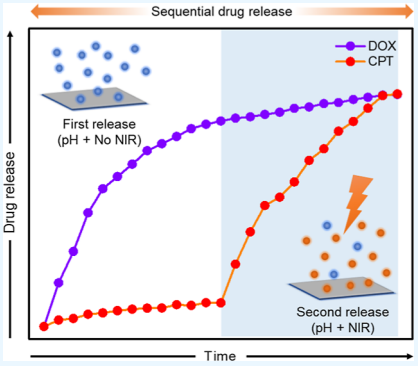

INTRODUCTION

Sequential drug delivery systems (DDS) show significant potential for enhancing the therapeutic effects of drugs. They are meant to manage the release of drugs/genes in a controlled manner based on a predetermined temporal or spatial sequence.[1−3] Because of the synergistic effects of genes and medications, this technique can potentially be a viable tool for extending gene expression periods, reducing drug side effects, and inhibiting the proliferation of cancer cells.[4−6] Multidrug regimens that include conventional medications can be systematically used to treat some complex medical diseases.[7,8] The majority of current platforms, however, suffer from several shortcomings, including biological distribution, dosage control, bioavailability, extreme toxicity, and inadequate drug efficacy, particularly in the case of treatments involving drugs that are insoluble in water or susceptible to decomposition.[2,9−11] To overcome these difficulties, several local DDSs are being constructed using polymer thin coatings, microfabricated devices, and nanoengineered drug-eluting inserts.[12−14]

Using controlled and sequenced release mechanisms to prevent undesirable outcomes associated with simultaneous codelivery, local DDSs can restrict drug−drug interactions, improve therapeutic effectiveness, and minimize drug resistance in skin cancer treatment.[15−17] The field of sequential and on-demand DDSs has seen a growth in the development of responsive biomaterials with configurable physical and chemical characteristics.[18−20] Because of their reversible phase transformation in reaction to stimulation and physiochemical influences such as pH, temperature, and enzymatic activity, and external forces such as UV light, near-infrared (NIR), ultrasound, electric, and magnetic radiation, these materials can be used as drug-carrier frameworks for the effective delivery of pharmaceuticals.[21−26] Because most drugs must be given repeatedly and consistently over long periods of time to be effective, and their concentrations must remain within the desired effective range to prevent overuse or underdosing, it is necessary to develop and improve new adaptive systems that can be easily controlled externally and capable of being spatially programmed.[5,27,28]

Drug toxicity in living cells and the maintenance of a minimal concentration of pharmaceuticals in the blood are the main goals of research on DDSs.[29−32] New strategies that enable controlled drug release are necessary considering these initiatives. Owing to the wide range of biomaterial properties, the application of layer-by-layer (LbL) films to DDSs has become a promising approach.[15,33] Polymers and different functional therapeutics or nanomaterials can be used to create these films.[34] LbL is a versatile manufacturing approach used extensively in hydrodynamic assembly conditions to provide functional surface coatings.[35] In LbL assembly, the substitution

Received: October 13, 2023
Revised: November 22, 2023
Accepted: November 24, 2023
Published: December 5, 2023

https://doi.org/10.1021/acsomega.3c08009
ACS Omega 2023, 8, 48405−48412

synthesis of diverse compounds with covalent interactions forms a multilayered structure.[36] LbL assembly is typically driven by electrostatic interactions between compounds with opposite charges. Multilayer films can significantly increase drug loading because of the presence of multivalent bonds with each component of the film.[37,38] Ionic binding allows charged pharmaceuticals to join ionized moieties on the film.[38] Hence, LbL films enable efficient drug integration and regulate drug release.

NIR irradiation has greatly enhanced cancer treatment because it penetrates deeply without severely damaging the surrounding cells and is only slightly absorbed by the skin and tissues in the range of 650−900 nm.[39−42] The tunable longitudinal absorption spectrum of gold nanorods (GNRs) in the NIR region makes them an appealing photothermal nanoagent for various therapeutic applications.[43−46] In addition, a drug can be stored in compartments created by the easily modifiable surface of GNRs. Drug-containing GNRs irradiated with NIR generate localized heat and vibrations that can result in on-demand drug release.[23,40,47] In this way, photoresponsive DDSs that allow precise spatiotemporal drug release at the desired sites of action can be developed.

In this study, we developed a novel LbL film platform loaded with two drugs: positively charged doxorubicin (DOX) in the layers and camptothecin (CPT) loaded onto the GNRs. The first layer was composed of linear polyethylenimine (LPEI), a polycation, and the positively charged surface of the layer was compensated by poly(sodium-4-styrenesulfonate) (PSS), a polyanion.[48] Initially, DOX was released to a limited extent at pH 7.4, while a more significant release was observed at pH 6. CPT and DOX were then sequentially released after NIR irradiation. While DOX release depends on the pH, CPT release depends on the local heat and vibration that NIR irradiation causes on the GNRs, which disrupt the interactions of C_{16}-PEG-CPT-GNRs. The current study offers a customizable framework for the scheduled, sequential, and safe drug delivery to target sites for treating topical dermatologic ailments.

EXPERIMENTAL SECTION

Materials. Polyethylene glycol (PEG)-2000, hexadecanol, triethylamine, methanesulfonyl chloride (98%), and PSS were purchased from Sigma-Aldrich (Seoul, South Korea). To produce the ligands, additional organic solvents were purchased from Sigma-Aldrich. CPT and DOX were purchased from TCI (Tokyo, Japan). LPEI was purchased from Alfa Aesar (Tewksbury, MA, USA). To obtain ^{1}H NMR spectra, the solvent $CDCl_3$ and a JEOL ECX-400 400 MHz spectrometer (JEOL, Tokyo, Japan) were utilized. Cells were obtained from the Korean Cell Line Bank (Seoul, South Korea). All cell studies-related supplies were bought according to our earlier study.[44] A QM-400 spectrophotometer (Horiba Scientific, Piscataway, NJ, USA) was used to obtain the fluorescence spectra. UV−vis absorption spectra were obtained using a Neosis-2000 UV/vis spectrophotometer (Sinco America, Twin Lakes, WI, USA). Temperature traces were captured using a Ti95 infrared camera (Fluke, Everett, WA, USA) and photostimulation was performed using an 808 nm diode laser system. A microplate reader (Tecan Trading AG, Mandorf, Switzerland) was used for the 3-(4,5-dimethylthiazolyl-2)-2,5-diphenyltetrazolium bromide (MTT) assay.

Preparation of LbL Films. The silicon substrate was negatively charged and activated after exposure for 5 min to oxygen plasma. Before constructing the LbL, the base layer was applied to the substrate by alternately depositing 10 bilayers of LPEI and PSS. In the LbL assembly approach, LPEI, PSS, C_{16}-PEG-CPT-GNRs, and DOX were used to develop an LbL film. The concentrations of LPEI, PSS, and DOX were 2 mg/mL. The LPEI and PSS solutions had a pH of 4.5, whereas the C_{16}-PEG-CPT-GNRs and DOX solutions had a pH of 7.0. The negatively charged silicon substrate was initially submerged in the LPEI fluid for 5 min, rinsed for 20 s with a medium maintained at the same pH as the solution used, and allowed to air-dry. The substrate was then washed and dried after incubation for 5 min in a solution of C_{16}-PEG-CPT-GNRs. After rinsing in water for 20 s, the substrate was submerged in the LPEI solution, washed, and dried to balance the negative charge of the preceding layer. The film was cleaned and dried by dipping in the DOX and PSS solutions to balance the positive charge of DOX after the initial drug loading was completed. Washing and drying were performed at each step. To prepare LbL films loaded with two drugs, a total of 20 bilayers comprising $(LPEI/C_{16}\text{-PEG-CPT-GNRs})_{10}$ and $(PSS/DOX)_{10}$ were deposited between the washing processes. The surface roughness of the films was evaluated using scanning electron microscopy (SEM), and the film thickness was measured using a profilometer.

Investigation of Sequential Drug Release. We assessed the sequential drug release dynamics of pH- and NIR-responsive LbL films loaded with layers of DOX and CPT confined by GNRs. The initial drug (DOX) release test was performed at pH 7.4 and 6. The second drug (CPT) was released by positioning the sample beneath the focus point of the illumination probe and exposing it to a diode laser (808 nm) operating at 1.6 W/cm^2 for 240 min over 10 min intervals to assess the drug release rate. Every 10 min, the same sample vessel was subjected to fluorescence spectroscopy to verify the drug release. Pulsatile drug release was conducted using a cyclical on−off method for 120 min of 10 min without light and 10 min of 1.6 W/cm^2 irradiation. Three samples with the same amount of drug were used in each drug release experiment, which was conducted at room temperature.

Assessment of Biocompatibility. This study employed an LbL film with only base layers, no drugs, and no further polyelectrolyte layers; hence, they were not subjected to NIR irradiation. B16−F10 melanoma cells were plated in 24-well plates at a density of $5 \times 1 \times 10^3$ cells/well. Before labeling, the LbL film was applied to the cell clusters for 24 and 48 h to ascertain whether the cells were alive or dead. Propidium iodide (PI) and fluorescein diacetate (FDA) were used to stain the live and dead cells, respectively.

Cellular Uptake. B16−F10 melanoma cells were also used to test the effectiveness of systemic drug delivery for drug absorption. In this experiment, calcein and rhodamine B (RhB) were used in the film layers instead of CPT and DOX. The resulting LbL film was placed on top of the cells cultured in a 24-well plate at an initial density of 5×10^3 cells/well. The experiment was performed with 1.6 W/cm^2 NIR illumination for 5 min without illumination.

Evaluation of Dug Loading Capacity and Efficiency. The drug loading capacity of GNRs was evaluated by preparing C_{16}-PEG-CPT-GNRs with different amounts of C_{16}-PEG during heterologous formation, which was calculated using the equation below

https://doi.org/10.1021/acsomega.3c08009
ACS Omega 2023, 8, 48405−48412

Scheme 1. Schematic Representation of a Light-Responsive LbL Film for the Sequential and On-Demand Release of Drugs

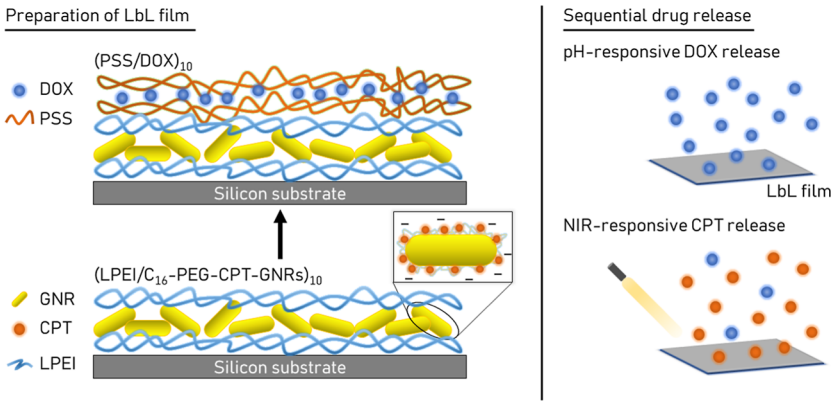

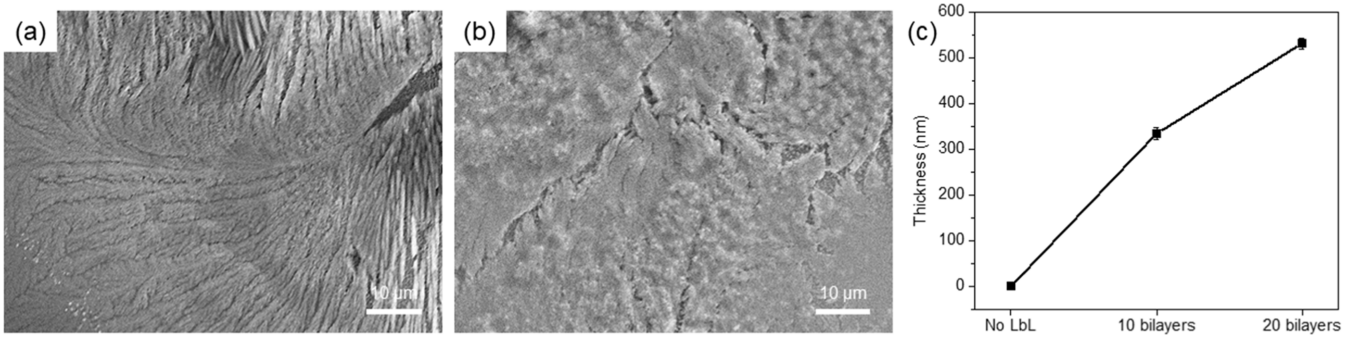

Figure 1. SEM images of LbL films containing (a) 10 bilayers and (b) 20 bilayers. (c) Measurement of the film thickness.

$$\text{Drug loading capacity (\%)} = \frac{\text{weight of drug on GNRs}}{\text{weight of GNRs recovered}} \times 100$$

Drug loading efficiency on LbL film was calculated by choosing different film size areas and different dipping times to form layers for both drugs (DOX and CPT) using the following equation

$$\text{Drug loading efficiency (\%)} = \frac{\text{weight of drug in LbL film}}{\text{weight of drug used in formulation}} \times 100$$

Data and Statistical Analysis. All numerical variables were subjected to statistical techniques, including means, standard deviations, and graphical analysis in OriginPro 8.5 software (OriginLab). For each experiment, the cell vitality was evaluated using three different samples from each group.

RESULTS AND DISCUSSION

LbL assembly is an ideal method of film fabrication for drug delivery because it does not restrict the size or shape of the substrate and does not require high temperatures or pressures. During the LbL fabrication process, multilayer films are formed on the surface of the substrate by alternate adsorption of the incorporated elements. Scheme 1 shows the composition of the LbL film used for sequential drug release by depositing oppositely charged components onto a pretreated silicon substrate. The prepared film displayed several properties, such as dual drug loading and sequential release in response to pH and NIR irradiation.

The two stages involved in synthesizing the final amphiphilic ligand C_{16}-PEG are depicted in Figure S1a. The prepared ligands were confirmed via NMR as follows: C_{16}-OMs: ^{1}H NMR (400 MHz, $CDCl_3$) δ-0.893 (t,3H), δ-1.250 (s, 26H), δ-1.692 (t, 2H) δ-3.061 (s, 3H) δ-4.237 (t, 2H). C_{16}-PEG: ^{1}H NMR (400 MHz, $CDCl_3$) δ-0.893 (t, 3H), δ-1.250 (s, 26H), δ-1.568 (t, 2H) δ-3.439 (t. 2H) δ-3.641 (s, 181H) (Figure S1b).

In this study, surface modification or functionalization is crucial. According to our earlier research, CTAB-GNRs prepared using the seed-mediated technique were functionalized with the cationic TMA ligand via a ligand-exchange process, generating TMA-GNRs.[44] This surface modification method is necessary for the subsequent conjugation of several compounds, including drugs and polymers. Physically encapsulating drugs in micelles of amphiphilic polymers has emerged as the best method for enhancing long-term stability, as the actual effects are reduced by chemically altering therapeutics using different covalent linkages. The electrostatic adsorption of the amphiphilic C_{16}-PEG containing CPT was facilitated by the strong cationic charge of the TMA-GNRs. After each surface alteration, the optical, electrical, and morphological characteristics of the GNRs were examined using UV−vis spectroscopy, zeta potential analysis, and transmission electron microscopy (TEM). The prevalent LSPR peaks of the original CTAB-GNRs at 520 and 734 nm are shown in Figure S2a. Both peaks generally retained their shape and SPR after the synthesis of cationic TMA-GNRs and, subsequently, C_{16}-PEG-CPT-GNRs. The original optical quality was also preserved, with high absorption at 808 nm, despite some redshift and broadening. Zeta potential evaluation confirmed that these surface transformations were

https://doi.org/10.1021/acsomega.3c08009
ACS Omega 2023, 8, 48405−48412

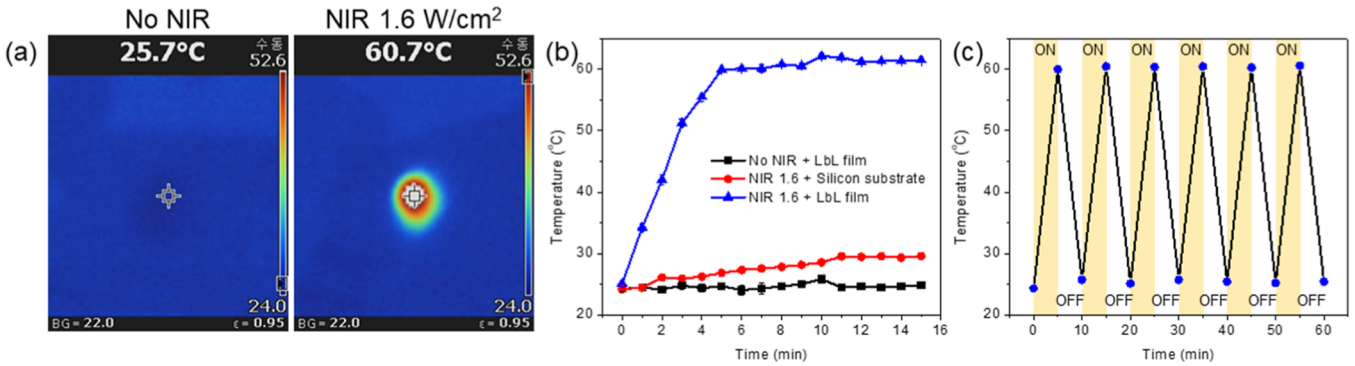

Figure 2. (a) Infrared images and (b) temperature changes in the LbL films under different conditions. (c) Thermal efficiency of the LbL film upon cyclic on−off NIR irradiation.

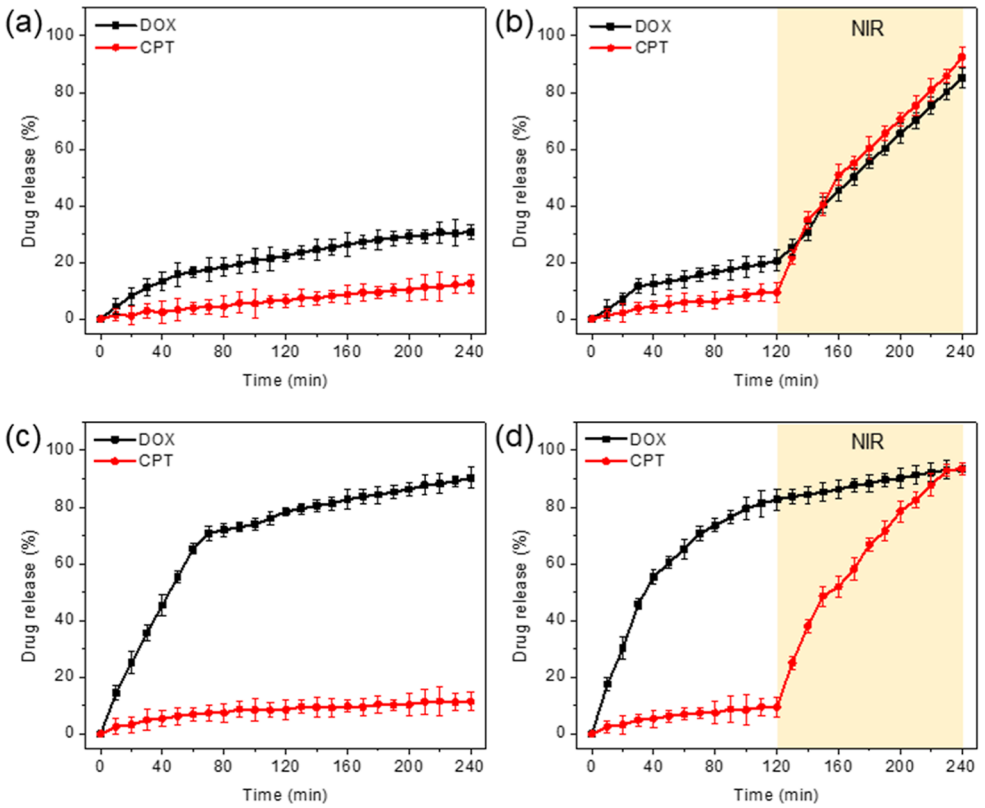

Figure 3. Sequential and on-demand drug release at (a,b) pH 7.4 and (c,d) pH 6 in the presence or absence of NIR light.

successful. CTAB-GNRs and TMA-GNRs had comparable positive zeta potentials of 42.7 and 25.3 mV, respectively (Figure S2b). However, the zeta potential of the C_{16}-PEG-CPT-GNRs was −35.5 mV, confirming that the CPT-loaded C_{16}-PEG moiety was properly attached to the surface of the GNRs. Additionally, TEM was used to confirm the morphology of CTAB-GNRs, TMA-GNRs, and C_{16}-PEG-CPT-GNRs (Figure S2c−e). Our approach successfully loaded CPT onto the GNRs using an amphiphilic C_{16}−PEG network.

The LbL film was also characterized to confirm its successful preparation and suitability for further experiments. The surfaces of the samples varied depending on the preparation technique used and the procedures involved in layer deposition. The acquired SEM images demonstrated that the surface became denser as the number of layers increased. After forming the base layers, a total of 20 bilayers were introduced $(LPEI/C_{16}\text{-PEG-CPT-GNRs})_{10}$ as shown in Figure 1a and $(LPEI/C_{16}\text{-PEG-CPT-GNRs})_{10}/(PSS/DOX)_{10}$ in Figure 1b, increasing the surface roughness. The overall configuration of the LbL assembly, which may be altered based on the medical application, and film thickness, which fluctuates at different phases of layer deposition, are essential parameters. The thickness and roughness of the LbL films were then assessed to confirm their successful fabrication. Figure 1c demonstrates that the film thickness increased to 334.6 and 531.3 nm at 10 and 20 bilayers, respectively.

NIR irradiation has many applications as an alternative tool to improve treatment outcomes and control drug delivery. The thermal effect on the film was further studied by subjecting it to NIR irradiation. After 5 min of NIR irradiation, the LbL film containing GNRs had a significant temperature increase of up to 60.7 °C; the film exhibited a temperature decrease of 25.7 °C when the light was turned off (Figure 2a). As shown in Figure 2b, temperature control of the LbL film in the presence

https://doi.org/10.1021/acsomega.3c08009
ACS Omega 2023, 8, 48405−48412

and absence of NIR was confirmed, and the temperature of the silicon substrate without layers upon NIR irradiation was examined. We observed that the temperature of the LbL film was higher upon NIR irradiation than that without NIR irradiation, while the temperature of the silicon substrate reached 29 °C after 15 min of NIR irradiation. An on−off strategy was employed to assess the thermal effectiveness of the cyclic process. This process was performed in cycles of 5 min with NIR irradiation (on) and 5 min without NIR irradiation (off), using 1.6 W/cm^2 laser power. The temperature of the LbL film increased to 60 °C when the NIR light was applied; the temperature decreased gradually in every cycle when the NIR light was turned off (Figure 2c).

The systematic release of therapeutics from the LbL film was investigated using a fluorescence spectroscopy device (Figure 3). Sequential drug release was observed in the LbL film samples measuring 1 cm. Both drugs exhibited controlled release and sequential properties. When exposed to NIR light, DOX and CPT exhibited variable release kinetics at different pH values. Without NIR exposure, DOX was released at rates of 30.7 ± 2.6% at pH 7.4 and 90.3 ± 3.7% at pH 6 over 240 min (Figure 3a,c). Meanwhile, less CPT was released but had a consistent release trend in both pH ranges. CPT was released at rates of 92.5 ± 3.3% at pH 7.4 and 93.5 ± 2.1% at pH 6 when the film was subjected to NIR illumination at an intensity of 1.6 W/cm^2, whereas DOX was released at rates of 85.1 ± 3.6% at pH 7.4 and 93.3 ± 2.0% at pH 6 (Figure 3b,d). NIR exposure does not affect the release of DOX at pH 6 because most of the amount of DOX has been released due to the acidic condition before irradiating NIR light; hence, a very modest release of DOX and saturation point can be observed after NIR exposure. On the other hand, we can see a significant increase in DOX with CPT due to NIR irradiation at pH 7.4. Hence, the film demonstrated dual-stimulus-responsive drug release in a sequential pattern with the addition of GNRs to the LbL assembly, indicating a viable on-demand drug delivery platform. This platform can regulate the medication release patterns and administration times by selecting different release segments.

To confirm the ability of the film for pulsatile drug release and to tolerate multiple treatments (Figure 4), we further examined the drug release profile upon on−off NIR irradiation. For the initial 120 min without NIR irradiation, DOX was continuously released at pH 6, whereas less CPT was released. After 120 min, the film was exposed to NIR laser irradiation for 10 min (on) followed by 10 min of nonexposure (off). Although there was no significant change in DOX release with or without NIR exposure, CPT release significantly improved in the presence and absence of NIR radiation in this experiment: 95.3 ± 2.3% of DOX and 95.5 ± 2.3% of CPT were released.

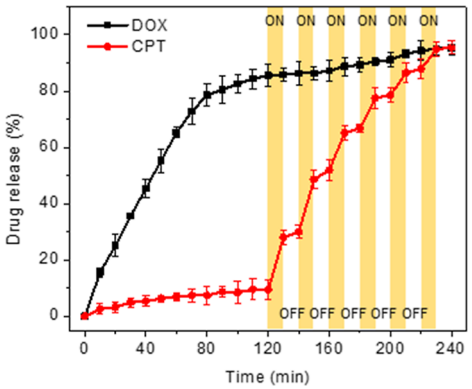

Figure 4. Drug release through a cyclic on−off process of NIR irradiation.

Only the base layers of the films were used to assess their biocompatibility and toxicological potential. Briefly, the cells were attached to the film and allowed to spread. The cells survived after 24 and 48 h (Figure 5). The presence of adherent cells confirms that the film promotes cell proliferation. The detection of green fluorescence (live cells) confirmed successful FDA labeling, and the cells retained their original orientation. However, PI staining revealed no red fluorescence (dead cells). After 48 h, the cells began to condense, indicating that the film had no cytotoxic effects (Figure 5d−f).

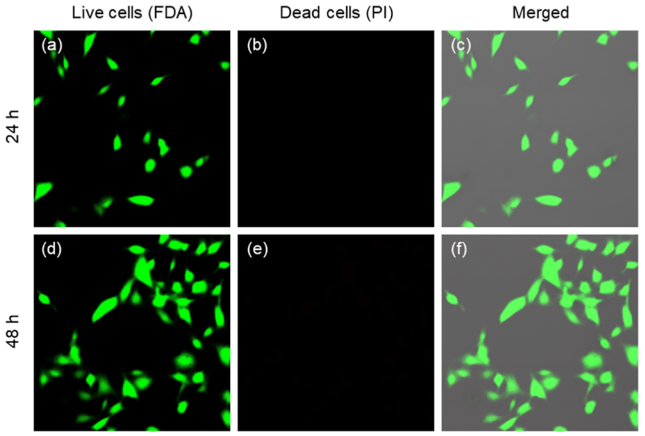

Figure 5. CLSM images of the biocompatibility assessment of LbL films showing cell growth at (a−c) 24 h and (d−f) 48 h before staining, as well as live−dead staining with FDA and propidium iodide (PI).

Cellular uptake was evaluated after 24 h of culturing 5 × 10^3 cells/well in a 24-well plate. Dyes were used to form the LbL films, substituting RhB for DOX and calcein for CPT. RhB and calcein were delivered continuously, and their cellular absorption was measured utilizing CLSM in the presence and absence of NIR light. Without exposure to NIR light, the LbL film delivered RhB (Figure 6a−c). Calcein fluorescence was not visible within the cells, but RhB fluorescence was observed (Figure 6b). The dye-loaded LbL films were then incubated for 2 h after exposure to laser light at an intensity of 1.6 W/cm^2 for up to 5 min. The successive discharge of dyes under NIR irradiation was illustrated by the fluorescence of RhB and calcein inside the cells (Figure 6d−f).

The effectiveness of our treatment strategy was investigated using the MTT assay and cell viability studies using B16−F10 melanoma cells. Briefly, the cells were grown in an incubator with 5% CO_2 for 24 h prior to the experiments. Cell damage was assessed in response to NIR irradiation without the LbL film or drugs. A slight decrease in cell viability was observed as the NIR light intensity increased, as shown in Figure 7a. Cell viability was assessed at all light intensity levels after incubation for 24 and 48 h of incubation. After incubation for 24 h, a significant decrease in cell viability was observed, dropping to 86.2 ± 2.3%, 81.0 ± 3.6%, and 68.2 ± 7.07%, respectively, with the discharge of DOX after immersion of the LbL film for 1, 5,

https://doi.org/10.1021/acsomega.3c08009
ACS Omega 2023, 8, 48405−48412

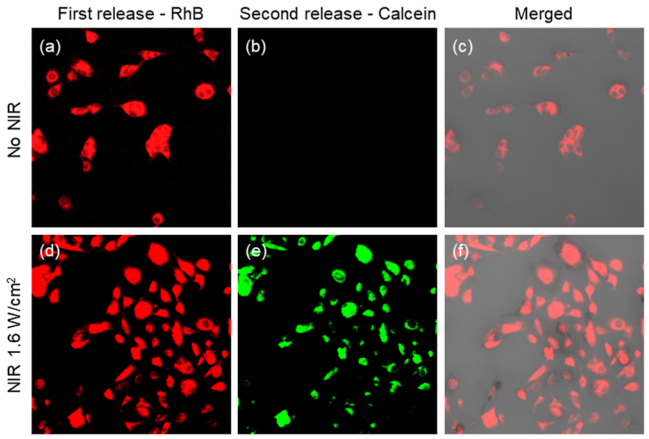

Figure 6. Cellular uptake (a–c) before and (d–f) after 5 min of NIR irradiation (1.6 W/cm^2).

and 10 min, respectively. However, after 48 h of incubation, the cell viability dropped to 60.0 ± 5.7%, 49.9 ± 0.6%, and 41.9 ± 3.8% after immersing the film for 1, 5, and 10 min, respectively (Figure 7b). In contrast, the anticancer properties of the LbL films were strengthened by the discharge of CPT after 1, 5, and 10 min of NIR irradiation. Maximum cell death was achieved 24 h after the discharge of CPT with the subsequent release of DOX, as the cell viability was reduced to 51.7 ± 4.7%, 44.7 ± 3.8%, and 32.4 ± 3.1% after immersion at 1, 5, and 10 min, respectively (Figure 7c). After 48 h, the cell viability was found to be 33.4 ± 3.1%, 25.4 ± 2.9%, and 10.7 ± 1.1% after film immersion for 1, 5, and 10 min, respectively. Figure 7d shows the amount of drug released from the LbL films at the indicated time intervals.

The drug loading capacity and efficiency of GNRs and LbL films, respectively, were evaluated. In Figure 8a, we can see that by increasing the amount of C_{16}-PEG, the drug loading capacity of the GNRs reached 88 ± 4.1%, and the loading efficiency of the LbL film was 83.5 ± 3.3% and 91 ± 4.8% for DOX and CPT, respectively, with 1 cm^2 of LbL film area (Figure 8b,c). According to these results, we can see that the loading capacity and efficiency can be optimized as required by changing the amount of chemicals, dipping time, and film area in the production. The drug dosage and payload used in this study are suitable to achieve our goal.

The LbL film was also used to test the methods for sequentially regulating the release of the two drugs. Our findings suggest topical multidrug delivery systems can be fabricated using LbL polymer-coated films. Polymer layer coatings can improve the drug-loading effectiveness of the film. The results of this study clearly support the potential use of this film as a therapeutic drug carrier. In addition, this customizable platform can be modified to provide the desired therapeutic outcome by precisely changing the approach and the environmental factors. There is significant promise for using this approach in the treatment of many complex disorders, including wound healing and skin malignancies.

CONCLUSIONS

In this study, we demonstrated a fast and simple method to fabricate LbL films, a robust nanoplatform consisting of multilayer polyelectrolytes, charge-based drugs, and drugs loaded onto GNRs deposited via electrostatic forces onto a preactivated silicon substrate, facilitating dual-drug loading. The changes in surface roughness, thickness, and temperature upon NIR irradiation confirmed the successful fabrication of the film and loading of the CPT-containing GNRs. The LbL film platform demonstrated excellent loading performance, simple preparation, and sequential drug delivery. Initially, DOX was released more easily at pH 6 than at pH 7.4. Following NIR irradiation under regulated circumstances, the release of CPT resulted from local heating and vibration, which

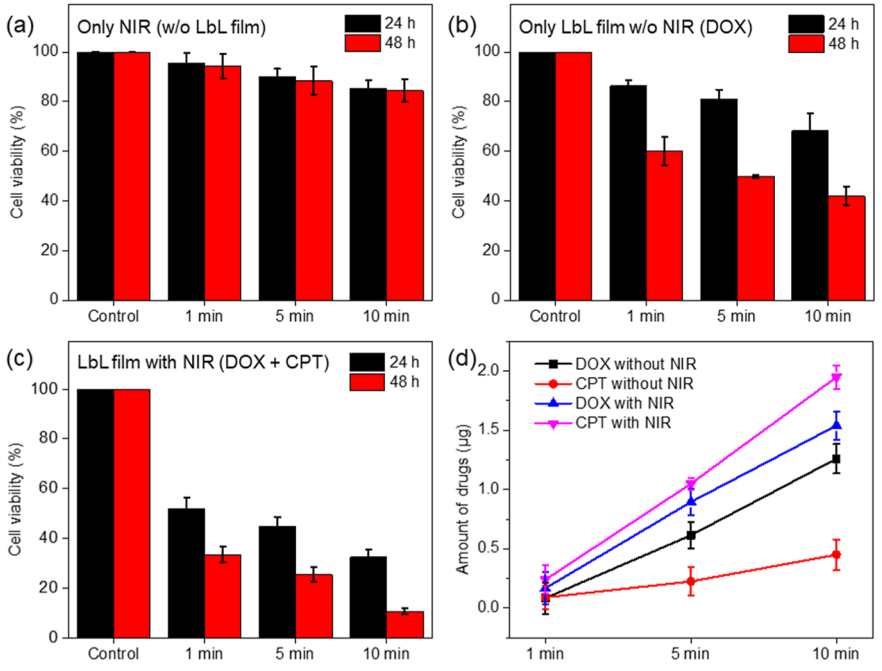

Figure 7. (a) The survival of cells upon NIR light exposure without the addition of LbL films. (b) Cell survival induced by DOX released from LbL films without NIR irradiation and (c) simultaneous release of DOX and CPT following NIR irradiation at the indicated intervals. (d) Quantification of the drugs released from the LbL film.

https://doi.org/10.1021/acsomega.3c08009
ACS Omega 2023, 8, 48405−48412

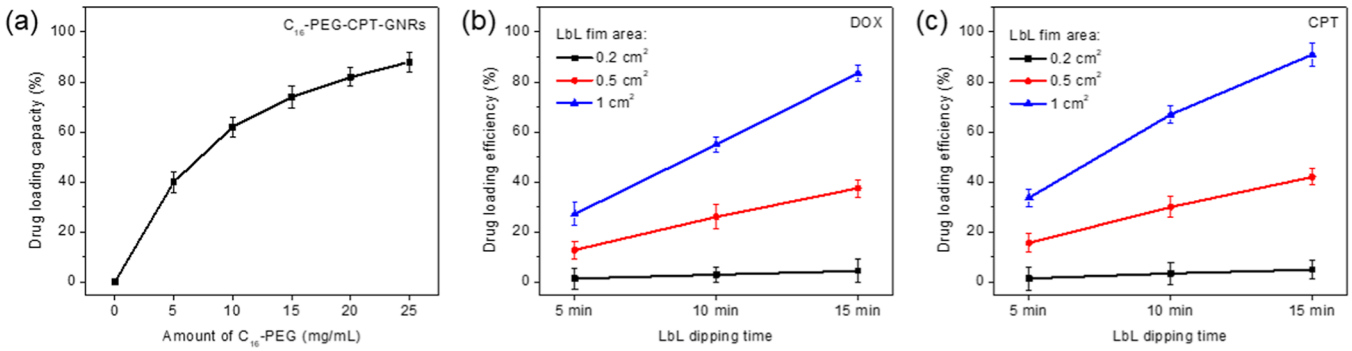

Figure 8. (a) Drug loading capacity of GNRs. (b) Drug loading efficiency of DOX and (c) CPT.

disturbed the entanglement of C_{16}-PEG-CPT-GNRs. Cell experiments demonstrated the good biocompatibility and anticancer properties of the film. Overall, the cytocompatibility, anticancer activity, and stimulus-responsiveness of this LbL film make it an excellent drug delivery platform.

■ ASSOCIATED CONTENT

Supporting Information

The Supporting Information is available free of charge at https://pubs.acs.org/doi/10.1021/acsomega.3c08009.

Additional experimental details, and methods of C_{16}-PEG synthesis, C_{16}-PEG-CPT-GNRs preparation, and MTT assay, including supplemental figures (PDF)

■ AUTHOR INFORMATION

Corresponding Author

Myoung-Hwan Park − *Department of Convergence Science, Sahmyook University, Seoul 01795, South Korea; Department of Chemistry and Life Science and Convergence Research Center, Nanobiomaterials Institute, Sahmyook University, Seoul 01795, South Korea; N to B Co., Ltd., Seoul 01795, South Korea;* orcid.org/0000-0003-3095-3016; Email: mpark@syu.ac.kr

Authors

Baljinder Singh − *Department of Convergence Science, Sahmyook University, Seoul 01795, South Korea;* orcid.org/0000-0001-8293-7718

Mamta Ramgopal Chejara − *Department of Convergence Science, Sahmyook University, Seoul 01795, South Korea*

Complete contact information is available at: https://pubs.acs.org/10.1021/acsomega.3c08009

Author Contributions

All authors have approved the final version of the manuscript.

Notes

The authors declare no competing financial interest.

■ ACKNOWLEDGMENTS

This study was funded by the Commercialization Promotion Agency for R&D Outcomes (grant numbers 2023-21040102-00 and 2023sanhagyeon-001).

■ ABBREVIATIONS

LbL, layer-by-layer; DDS, drug delivery system; GNRs, gold nanorods; NIR, near-infrared; CPT, camptothecin; DOX, doxorubicin; LPEI, linear polyethyleneimine; PSS, poly(sodium-4-styrenesulfonate); MTT, 3-(4,5-dimethylthiazolyl-2)-2,5-diphenyltetrazolium bromide; PEG, polyethylene glycol; TMA, HS-C_{11}-trimethylammonium; CTAB, cetyltrimethylammonium bromide; TEM, transmission electron microscopy; SEM, scanning electron microscope; UV−vis, ultraviolet−visible; TLC, thin layer chromatography; NMR, nuclear magnetic resonance

■ REFERENCES

(1) Guo, H.; Tan, S.; Gao, J.; Wang, L. Sequential Release of Drugs Form a Dual-Delivery System Based on Ph-Responsive Nanofibrous Mats Towards Wound Care. *J. Mater. Chem. B* **2020**, *8*, 1759−1770.

(2) Jana, B.; Kim, D.; Choi, H.; Kim, M.; Kim, K.; Kim, S.; Jin, S.; Park, M. H.; Lee, K. H.; Yoon, C.; Lee, B. S.; Kang, M. S.; Lim, H. J.; Park, E. J.; Jeong, Y.; Ryu, J. H.; Kim, C. Drug Resistance-Free Cytotoxic Nanodrugs in Composites for Cancer Therapy. *J. Mater. Chem. B* **2021**, *9*, 3143−3152.

(3) Doddapaneni, B. S.; Al-Fatease, A. M.; Rao, D. A.; Alani, A. W. G. Dual-Drug Loaded Micelle for Combinatorial Therapy Targeting Hif and Mtor Signaling Pathways for Ovarian Cancer Treatment. *J. Controlled Release* **2019**, *307*, 272−281.

(4) Xiao, B.; Si, X.; Han, M. K.; Viennois, E.; Zhang, M.; Merlin, D. Co-Delivery of Camptothecin and Curcumin by Cationic Polymeric Nanoparticles for Synergistic Colon Cancer Combination Chemotherapy. *J. Mater. Chem. B* **2015**, *3*, 7724−7733.

(5) Zhu, F.; Tan, G.; Zhong, Y.; Jiang, Y.; Cai, L.; Yu, Z.; Liu, S.; Ren, F. Smart Nanoplatform for Sequential Drug Release and Enhanced Chemo-Thermal Effect of Dual Drug Loaded Gold Nanorod Vesicles for Cancer Therapy. *J. Nanobiotechnol.* **2019**, *17*, 44.

(6) Li, J.; Xu, W.; Li, D.; Liu, T.; Zhang, Y. S.; Ding, J.; Chen, X. Locally Deployable Nanofiber Patch for Sequential Drug Delivery in Treatment of Primary and Advanced Orthotopic Hepatomas. *ACS Nano* **2018**, *12*, 6685−6699.

(7) Aw, M. S.; Addai-Mensah, J.; Losic, D. A Multi-Drug Delivery System with Sequential Release Using Titania Nanotube Arrays. *Chem. Commun.* **2012**, *48*, 3348−3350.

(8) Chen, M.; Tian, J.; Liu, Y.; Cao, H.; Li, R.; Wang, J.; Wu, J.; Zhang, Q. Dynamic Covalent Constructed Self-Healing Hydrogel for Sequential Delivery of Antibacterial Agent and Growth Factor in Wound Healing. *Chem. Eng. J.* **2019**, *373*, 413−424.

(9) Kim, K.; Jo, M. C.; Jeong, S.; Palanikumar, L.; Rotello, V. M.; Ryu, J. H.; Park, M. H. Externally Controlled Drug Release Using a Gold Nanorod Contained Composite Membrane. *Nanoscale* **2016**, *8*, 11949−11955.

(10) Liao, Z.; Tu, L.; Li, X.; Liang, X.-J.; Huo, S. Virus-Inspired Nanosystems for Drug Delivery. *Nanoscale* **2021**, *13*, 18912−18924.

(11) Senapati, S.; Mahanta, A. K.; Kumar, S.; Maiti, P. Controlled Drug Delivery Vehicles for Cancer Treatment and Their Performance. *Signal Transduction Targeted Ther.* **2018**, *3*, 7.

(12) Fu, Y.; Chen, X.; Mou, X.; Ren, Z.; Li, X.; Han, G. A Dual-Color Luminescent Localized Drug Delivery System with Ratio-

metric-Monitored Doxorubicin Release Functionalities. *ACS Biomater. Sci. Eng.* **2016**, *2*, 652−661.
(13) Singh, B.; Kim, J.; Shukla, N.; Lee, J.; Kim, K.; Park, M.-H. Smart Delivery Platform Using Core-Shell Nanofibers for Sequential Drug Release in Wound Healing. *ACS Appl. Bio Mater.* **2023**, *6*, 2314−2324.
(14) Park, H.; Yang, S.; Kang, J. Y.; Park, M. H. On-Demand Drug Delivery System Using Micro-Organogels with Gold Nanorods. *ACS Med. Chem. Lett.* **2016**, *7*, 1087−1091.
(15) Cheng, G.; Yin, C.; Tu, H.; Jiang, S.; Wang, Q.; Zhou, X.; Xing, X.; Xie, C.; Shi, X.; Du, Y.; Deng, H.; Li, Z. Controlled Co-Delivery of Growth Factors through Layer-by-Layer Assembly of Core-Shell Nanofibers for Improving Bone Regeneration. *ACS Nano* **2019**, *13*, 6372−6382.
(16) Adepu, S.; Ramakrishna, S. Controlled Drug Delivery Systems: Current Status and Future Directions. *Molecules* **2021**, *26*, 5905.
(17) Zhang, L.; Su, H.; Liu, Y.; Pang, N.; Li, J.; Qi, X. R. Enhancing Solid Tumor Therapy with Sequential Delivery of Dexamethasone and Docetaxel Engineered in a Single Carrier to Overcome Stromal Resistance to Drug Delivery. *J. Controlled Release* **2019**, *294*, 1−16.
(18) Safdar, M.; Ozaslan, M.; Junejo, Y.; Channa, I. S. Cytotoxic and Anticancer Activity of a Novel Synthesized Tet-Aunps Simultaneously Activates P53 and Inhibits Nf-Kb Signaling in Skbr3 Cell Line. *Toxicol. Environ. Health Sci.* **2021**, *14*, 69−76.
(19) Ahmad, T.; McGrath, S.; Sirafim, C.; do Amaral, R.; Soong, S. L.; Sitram, R.; Turkistani, S.; Santarella, F.; Kearney, C. J. Development of Wound Healing Scaffolds with Precisely-Triggered Sequential Release of Therapeutic Nanoparticles. *Biomater. Sci.* **2021**, *9*, 4278−4288.
(20) Cho, C.-H.; Shin, H.-J.; Singh, B.; Kim, K.; Park, M.-H. Assessment of Sub-200-Nm Nanobubbles with Ultra-High Stability in Water. *Appl. Water Sci.* **2023**, *13*, 149.
(21) Liu, H.; Fu, Y.; Li, Y.; Ren, Z.; Li, X.; Han, G.; Mao, C. A Fibrous Localized Drug Delivery Platform with Nir-Triggered and Optically Monitored Drug Release. *Langmuir* **2016**, *32*, 9083−9090.
(22) AlSawaftah, N. M.; Awad, N. S.; Pitt, W. G.; Husseini, G. A. Ph-Responsive Nanocarriers in Cancer Therapy. *Polymers* **2022**, *14*, 936.
(23) Yang, S.; Palanikumar, L.; Jeong, S.; Kim, K.; Lee, J.; Jeoung, E.; Kim, C.; Ryu, J.-H.; Park, M.-H. Synergistic Effect of Photothermal Therapy and Chemotherapy Using Camptothecin-Conjugated Gold Nanorods. *Part. Part. Syst. Char.* **2018**, *35*, 1700307.
(24) Fang, J. H.; Lai, Y. H.; Chiu, T. L.; Chen, Y. Y.; Hu, S. H.; Chen, S. Y. Magnetic Core-Shell Nanocapsules with Dual-Targeting Capabilities and Co-Delivery of Multiple Drugs to Treat Brain Gliomas. *Adv. Healthcare Mater.* **2014**, *3*, 1250−1260.
(25) Kim, H.-G.; Yu, Y. W.; Yang, Y.; Park, M.-H. Portable Environmental Microfluidic Chips with Colorimetric Sensors: Image Recognition and Visualization. *Toxicol. Environ. Health Sci.* **2019**, *11*, 320−326.
(26) Singh, B.; Lee, J.; Kim, H.-G.; Park, M.-H.; Kim, K. Colorimetric Detection of Copper Ions Using Porphyrin-Conjugated Silica Nanoparticles. *Toxicol. Environ. Health Sci.* **2020**, *12*, 381−389.
(27) Kim, J.; Singh, B.; Shukla, N.; Lee, J.; Kim, K.; Park, M.-H. On-Demand Drug-Delivery Platform Using Electrospun Nanofibers by Externally Triggered Glass Transition Switch. *ACS Mater. Lett.* **2022**, *4*, 2252−2260.
(28) Wu, H.; Tang, Z.; You, R.; Pan, S.; Liu, W.; Zhang, H.; Li, T.; Yang, Y.; Sun, C.; Pang, W.; et al. Manipulations of Micro/Nanoparticles Using Gigahertz Acoustic Streaming Tweezers. *Nanotechnol. Precis. Eng.* **2022**, *5*, 023001.
(29) Singh, B.; Kim, K.; Park, M. H. On-Demand Drug Delivery Systems Using Nanofibers. *Nanomaterials* **2021**, *11*, 3411.
(30) Xu, M.; Li, G.; Zhang, H.; Chen, X.; Li, Y.; Yao, Q.; Xie, M. Sequential Delivery of Dual Drugs with Nanostructured Lipid Carriers for Improving Synergistic Tumor Treatment Effect. *Drug Delivery* **2020**, *27*, 983−995.
(31) Venkatesan, H.; Soundhararajan, R.; Srinivasan, H. Interaction of Various Types of Bisphenols with Enzymes Involved in Melanin Synthesis. *Toxicol. Environ. Health Sci.* **2022**, *14*, 19−24.
(32) Fu, Y.; Li, X.; Ren, Z.; Mao, C.; Han, G. Multifunctional Electrospun Nanofibers for Enhancing Localized Cancer Treatment. *Small* **2018**, *14*, No. e1801183.
(33) Huang, R.; Li, W.; Lv, X.; Lei, Z.; Bian, Y.; Deng, H.; Wang, H.; Li, J.; Li, X. Biomimetic Lbl Structured Nanofibrous Matrices Assembled by Chitosan/Collagen for Promoting Wound Healing. *Biomaterials* **2015**, *53*, 58−75.
(34) Chauhan, N.; Saxena, K.; Tikadar, M.; Jain, U. Recent Advances in the Design of Biosensors Based on Novel Nanomaterials: An Insight. *Nanotechnol. Precis. Eng.* **2021**, *4*, 045003.
(35) Liu, R.; Dai, J.; Ma, L.; Chen, J.; Shi, X.; Du, Y.; Li, Z.; Deng, H. Low-Temperature Plasma Treatment-Assisted Layer-by-Layer Self-Assembly for the Modification of Nanofibrous Mats. *J. Colloid Interface Sci.* **2019**, *540*, 535−543.
(36) Alkekhia, D.; Hammond, P. T.; Shukla, A. Layer-by-Layer Biomaterials for Drug Delivery. *Annu. Rev. Biomed. Eng.* **2020**, *22*, 1−24.
(37) Park, S.; Han, U.; Choi, D.; Hong, J. Layer-by-Layer Assembled Polymeric Thin Films as Prospective Drug Delivery Carriers: Design and Applications. *Biomater. Res.* **2018**, *22*, 29.
(38) Rivero, P. J.; Goicoechea, J.; Arregui, F. J. Layer-by-Layer Nano-Assembly: A Powerful Tool for Optical Fiber Sensing Applications. *Sensors* **2019**, *19*, 683.
(39) Yu, H.; Ning, N.; Meng, X.; Chittasupho, C.; Jiang, L.; Zhao, Y. Sequential Drug Delivery in Targeted Cancer Therapy. *Pharmaceutics* **2022**, *14*, 573.
(40) Shukla, N.; Singh, B.; Kim, H. J.; Park, M. H.; Kim, K. Combinational Chemotherapy and Photothermal Therapy Using a Gold Nanorod Platform for Cancer Treatment. *Part. Part. Syst. Char.* **2020**, *37*, 2000099.
(41) Shalvi; Kumar, N.; Verma, K. L.; Jain, V. K.; Nagpal, S. Integrated Device for Colorimetric Detection of Arsenite Using Polyethylene Glycol Capped Gold Nanoparticles—Lab-on-Chip. *Toxicol. Environ. Health Sci.* **2021**, *13*, 351−362.
(42) Mohseni, H. s.; Sahebnasagh, R.; Tavajohi, S.; Ghahremani, M. H.; Kebriaeezadeh, A.; Aliebrahimi, S.; Ostad, S. N. Evaluation of Genotoxic and Cytotoxic Effects of Some Insecticides Used in Iran on Murine Fibroblast Cells (L-929). *Toxicol. Environ. Health Sci.* **2022**, *14*, 301−306.
(43) Dai, Y.; Bi, H.; Deng, X.; Li, C.; He, F.; Ma, P.; Yang, P.; Lin, J. 808 Nm near-Infrared Light Controlled Dual-Drug Release and Cancer Therapy in Vivo by Upconversion Mesoporous Silica Nanostructures. *J. Mater. Chem. B* **2017**, *5*, 2086−2095.
(44) Singh, B.; Shukla, N.; Kim, J.; Kim, K.; Park, M. H. Stimuli-Responsive Nanofibers Containing Gold Nanorods for on-Demand Drug Delivery Platforms. *Pharmaceutics* **2021**, *13*, 1319.
(45) Jeong, S.; Park, H.; Seon, D.; Choi, J.; Hong, K. B.; Lee, J.; Kim, C.; Kim, J. K.; Park, M. H. Modulatory Functionalization of Gold Nanorods Using Supramolecular Assemblies. *Chem.−Asian J.* **2017**, *12*, 2591−2596.
(46) Singh, B.; Shukla, N.; Cho, C.-H.; Kim, B. S.; Park, M.-H.; Kim, K. Effect and Application of Micro- and Nanobubbles in Water Purification. *Toxicol. Environ. Health Sci.* **2021**, *13*, 9−16.
(47) Yang, X.; Zhang, M. Review of Flexible Microelectromechanical System Sensors and Devices. *Nanotechnol. Precis. Eng.* **2021**, *4*, 025001.
(48) Singh, B.; Yun, S.; Park, M.-H. Light-Responsive Layer-by-Layer Assembled Nanofibers for Sequential Drug Release. *J. Drug Delivery Sci. Technol.* **2023**, *88*, 104910.

https://doi.org/10.1021/acsomega.3c08009
ACS Omega 2023, 8, 48405−48412